Sub-band Pairwise Coding for Robust Nyquist-WDM Superchannel Transmission

Chen Zhu, Binhuang Song, Leimeng Zhuang, Bill Corcoran, *Member*, *IEEE*,
and Arthur James Lowery, *Fellow*, *IEEE*

***Abstract*—Nyquist wavelength-division-multiplexed (N-WDM) coherent optical superchannel systems closely pack a set of rectangular-shaped channels, to realize high-spectral-efficiency transmission. In long-haul fiber links, dividing each of these channels into multiple sub-bands, each a few gigahertz wide, can increase tolerance to fiber nonlinearity. However, these low-bandwidth sub-bands will be sensitive to laser drift, which could cause them to overlap, creating inter-channel interference (ICI). In this paper, we propose applying pairwise pre-coding across the middle and edge sub-bands to improve their ICI tolerance. The proposed scheme is verified in super-channel experiments, and shows about 1.5-dB Q^2 improvement after 3840-km transmission for QPSK modulation and 1-dB Q^2 gain with 16-QAM modulation after 800-km transmission.**

***Index Terms*—Superchannel, inter-channel-interference, coherent optical communications, pairwise coding, Nyquist-WDM.**

I. Introduction

The exponentially increasing traffic demand for backbone network has been pushing the bit-rate-per-wavelength in optical transmission, from commercially available 100-Gb/s employing polarization-division-multiplexing quadrature phase shift keying (PDM-QPSK), towards 400-Gb/s or even 1-Tb/s [1], [2]. Although upgrading QPSK towards high-order quadrature-amplitude-modulation (QAM) formats is a straightforward way to realize such an increase, the achievable system reach decreases due to the denser constellations. Therefore superchannel techniques are attractive, since they enhance the spectrum efficiency by closely packing multiple spectrally shaped wavelength-division-multiplexed (WDM) channels, without loss of system sensitivity. Nyquist-WDM (N-WDM) superchannel systems [3]-[5] are promising candidates to support per wavelength baud rate approaching the channel spacing, because they guarantee the temporal orthogonality of each wavelength channel with inter-symbol-interference (ISI)-free sinc pulse shaping; inter-carrier-interference (ICI) is also controlled by shaping each channel's spectrum to have low side lobes. Moreover, several studies [6]-[8] have shown that a smaller per-channel symbol rate leads to a better nonlinear transmission performance for dispersion-unmanaged, long-haul links. As such, it is desirable to generate multiple sub-bands on each optical carrier when using commercial optical I/Q modulators that typically have 20-30 GHz bandwidths.

After long-haul fiber transmission, the ISI can be reduced by using powerful digital signal processing (DSP) to remove the linear fiber channel impairments. Conversely, the ICI is very sensitive to the drifts in the center frequencies of the closely-packed channels, and is not easy to remove by DSP. For per-channel reception, ICI behaves as additional random noise which is not possible to predict, therefore it is difficult to compensate for. Liu *et al.* [9] propose that by using the information from multiple channels at the receiver, joint processing can be performed to mitigate ICI. However, this approach requires precisely synchronized sampling of multiple channels using multiple receivers, and also heavy computational effort. Furthermore, if the channels are wavelength-routed during transmission, such that the *received* neighboring channels are not the sole source of ICI, the performance improvement for the scheme in [9] is limited. On the other hand, if multiple sub-bands are defined in each channel, ICI would mainly fall onto the edge sub-bands. In this case a larger detection penalty is expected on the edge sub-bands, because compared with a single sub-band case, each sub-band now has a narrower bandwidth, so is proportionally more sensitive to ICI.

This problem can be viewed as 'edge sub-band selective fading', which suggests that it can be overcome using fading mitigation methods. Many fading mitigation methods are available from wireless technology; for example, by assigning different modulation formats and powers onto different sub-bands [10], or by employing space-time pre-coding schemes [11], [12], the overall system bit error rate (BER) can be significantly improved. However, these bit- and power-loading techniques require the instantaneous signal-to-interference-and-noise ratio (SINR) to be fed back to the transmitter to achieve optimal performance, which could be difficult to achieve due to the fast and randomly varying nature of the ICI. Although space-time coding schemes could be applied without any prior knowledge, they need to

Issue No xxxxxxxxxxxxxx 2015.

All the authors are with the Electro-Photonics Laboratory, Department of Electrical and Computer Systems Engineering, Monash University, Australia (e-mail: {chen.zhu; binhuang.song; leimeng.zhuang; bill.corcoran; arthur.lowey} @ monash.edu). B. Corcoran and A. J. Lowery are also with the Centre for Ultrahigh-bandwidth Devices for Optical Systems (CUDOS), Australia. This work is supported under the Australian Research Council's Laureate Fellowship (FL130100041) and Centres of Excellence (CE110001018) schemes.

cooperate with the decoders, and this is computationally costly, so impractical.

Given these considerations, we need a technique that is able to provide an effective performance gain over a wide range of ICI values adaptively, without requiring feedback to the transmitter, and is also low in computational complexity.

In this paper, we propose employing sub-band pairwise coding to enhance the N-WDM system robustness against ICI. We have previously proposed pairwise coding [13] to improve the overall system performance with fading between sub-carriers of direction-detection orthogonal frequency division multiplexing (DDO-OFDM) systems due to non-uniform spectral distribution of signal-to-noise-ratio (SNR) [14]. We have also proposed pairwise coding to mitigate the penalty due polarization dependent loss (PDL) in polarization-division-multiplexed (PDM) systems [15]. Importantly, pairwise coding has: zero overhead, low-complexity pre-coding and decoding processes, reasonable performance enhancement with a fixed pre-coding structure over a wide range of fading values [16], and is computationally simple to implement.

This paper is based on our original PDM-QPSK N-WDM experiment presented at ECOC-2015 [17]. It has been extended including: a detail analysis of the coding theory, additional simulation and PDM-16-QAM N-WDM experimental results. By pairing the edge and middle sub-bands of each N-WDM channel with fixed pre-rotation angle, the penalties due to different ICI levels can be greatly reduced. The proposed method is demonstrated in superchannel experiments, with 16 N-WDM channels, each carrying four sub-bands, with different emulated laser drift induced ICIs. With 1-GHz channel overlap, 1.5-dB Q^2 improvement can be attained after 3840-km transmission for QPSK modulation, and about 1-dB Q^2 gain is realized for 16-QAM modulation.

II. Principle for Sub-Band Pairwise Coding

A. Theory of pairwise coding

The fundamental idea of pairwise coding originates from maximizing the detection performance for signals suffering different levels of in-phase and quadrature noise. This is achieved by rotating the transmitted constellations and rescaling the received signals' inphase (I) and quadrature (Q) components separately [18]. Figure 1 shows two simple examples. The transmitted signals have four constellation points, with unit power on both the real and the imaginary components. In Figs. 1(a)-(c), the SNR for the I and Q components are 6 and 10 dB, respectively. As shown in Fig. 1(a), transmitting a square 4-QAM results in the lowest Q^2-factor defined as: $Q^2(dB) = 20\log_{10}(\sqrt{2}erfc^{-1}(2BER))$. Fig. 1(b) is for signals transmitted with the square 4-QAM rotated by 45°; 0.46-dB improvement can be observed. In Fig. 1(c), the received real and imaginary components from Fig. 1(b) have been rescaled according to the I/Q SNR ratio λ (that is, multiplying the imaginary part by square root of $10^{0.4}$ when λ = 4 dB), then maximum likelihood detection has been performed based on the rotated and rescaled constellation points (red dots). For this case, a further 0.7-dB Q^2 improvement can be observed. The decision regions are shown

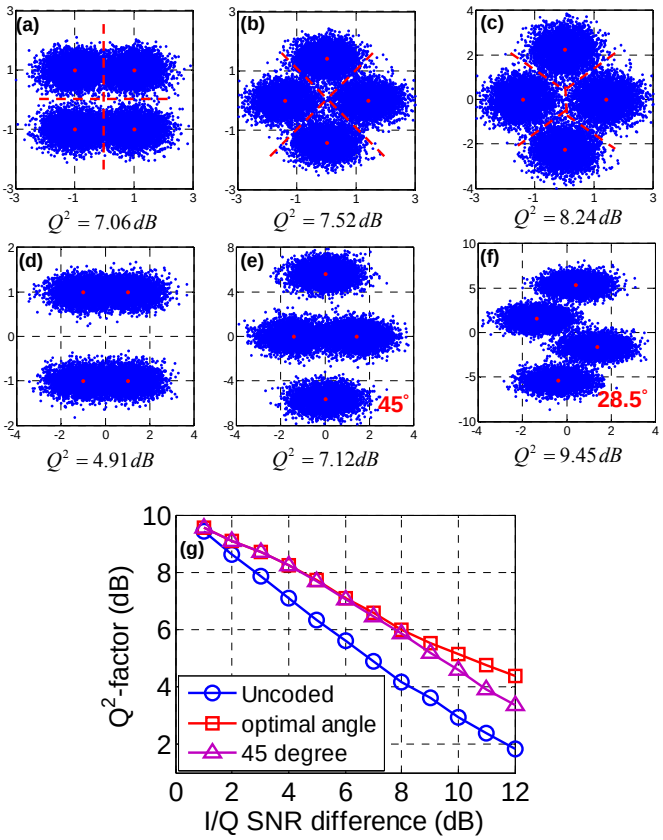

Fig. 1. Rotated and rescaled conventional constellations for performance improvement against imbalanced in-phase and quadrature noises. (a)-(c): 6- and 10-dB SNR (λ = 4-dB) on I and Q parts, (d)-(f): 3- and 15-dB SNR (λ = 12 dB) on I and Q parts, (g): fixed 10-dB SNR on Q and different SNR values on I.

in red dashed curves. Clearly this 'rotate + rescale' processes provides an improved decision region for signal detection.

Obviously the pre-rotation angle is the key parameter that determines the performance gain. Although the optimal rotation angle depends both on the total SNR and the λ [16], this angle can be well approximated using only the SNR ratio λ parameter [13]:

$$\theta_{opt} = \begin{cases} 45^\circ & \lambda \le 3 \\ \tan^{-1}[(\lambda-1) - \sqrt{(\lambda-1)^2 - \lambda} & \lambda > 3 \end{cases} \quad (1)$$

In Figs. 1(d)-(f), the SNR for I and Q components are set to 3- and 15-dB respectively. The rotation angles are set to 45° and 28.5° (optimal angle) for Figs. 1(e) and (f), respectively, providing 2.2- and 4.5-dB improvements in Q^2, compared with the square 4-QAM case. By comparing the constellations, the optimal angle provides equal overlaps between the four clusters in the constellation, while the detection errors are mainly due to the overlap of two clusters in the 45° case. However, since implementing the optimal angle at the transmitter requires the λ-value, which normally can only be found at the receiver, it is preferable to use a fixed rotation angle to avoid needing a feedback path. As 45° is the optimal angle when λ is less than 4.7-dB (i.e. < 3), it is a good choice if it is able to provide reasonable gain with other λ values. Figure 1(g) shows the performance with fixed 10-dB SNR on

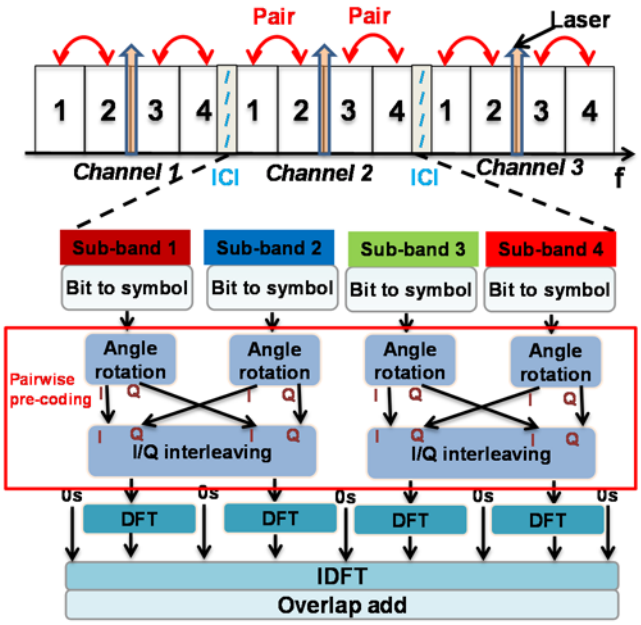

Fig. 2. Transmitter DSP for sub-band pairwise coding.

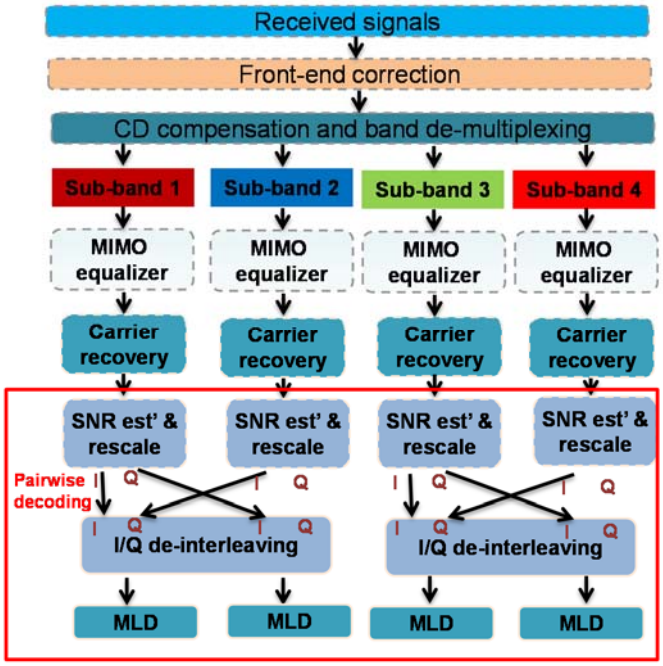

Fig. 3. Receiver DSP for sub-band pairwise coding.

imaginary part and -2 to 9 dB SNR on real part, $\theta = 45^{\circ}$ provides most of the performance gain, even when λ is larger than 4.7 dB, indicating that it is a good choice for a fixed rotation angle for various λ values. In the rest of the paper, the pre-rotation angle is fixed at 45° for the pairwise coded signals.

Pairwise coding is an application for the concept discussed. For two independent data streams, consider the case where one stream suffers deep 'channel fading', so has much poorer SNR (SINR) than the other stream. We can interleave the *I* and *Q* components between these two data streams at the transmitter, so that at the receiver, after de-interleaving, the fading becomes an *I*/*Q* SNR imbalance for both data streams. However, one should not mistake pairwise coding to the approach of averaging the noise between two data streams, because the constellation rotation and rescaling techniques are designed to maximize the system performance according to a particular fading value, whereas noise averaging does not employ diversity in the complex plane.

Consider an extreme case, where one data stream suffers noise and the other is noise-free. The bit and power loading scheme would abandon the noisy data stream and allocate all the transmit power to the noise free data stream to achieve infinite capacity. Pairwise coding is also analogous to this 'water filling' concept, *i.e.* 'filling' the constellation flexibly according to the distribution of noise between *I* and *Q*. So in this case, with pairwise coding, after receiver *I*/*Q* de-interleaving, both data streams would have either noise only on the real (or imaginary) component; the rescaling processing will change the decoded signal to be exactly identical to a pulse-amplitude-modulation (PAM) signal, with detection not dependent on the noise terms. This would achieve error-free detection.

B. Implementation of sub-band pairwise coding

Figure 2 shows the signal generation process of the proposed sub-band pairwise coding scheme. Each channel (with its own laser) contains four sub-bands, so edge sub-bands 1 and 4 would be affected by a random laser drift of several GHz, while the middle sub-bands 2 and 3 would remain almost unaffected. The digital generation of each channel is based on a multi-sub-band N-WDM generation technique [19]. Very small guard bands (e.g. 50 MHz guard band between 3-GHz sub-bands) are typically defined between the adjacent sub-bands to allow a perfect de-multiplexing at the receiver. After bit-to-symbol mapping, the adjacent edge and middle sub-bands are paired, and pre-coding is applied to these two sub-band pairs before the DFT operation. For each sub-band, a constant phase shift (i.e. angular rotation) is first applied to the data symbols. After this, the in-phase and quadrature components are interleaved to generate the signals for each sub-band:

$$\begin{aligned} \mathbf{Tx}_e &= \Re(\mathbf{T}_e \cdot \mathrm{e}^{j\phi}) + j\Re(\mathbf{T}_m \cdot \mathrm{e}^{j\phi}) \\ \mathbf{Tx}_m &= \Im(\mathbf{T}_e \cdot \mathrm{e}^{j\phi}) + j\Im(\mathbf{T}_m \cdot \mathrm{e}^{j\phi}) \end{aligned} \quad (1)$$

Where: $\mathbf{T}_e$ and $\mathbf{T}_m$ denote the original data symbols (e.g. QPSK) at edge and middle sub-bands, respectively, ϕ is the rotation angle, and $\mathbf{Tx}_e$ and $\mathbf{Tx}_m$ represent the coded signals at edge and middle sub-bands, respectively. Then, after band mapping, an IDFT converts the signal to the time domain, the subsequent overlap-add is used to create a continuous signal by spreading the samples across the IDFT boundaries.

The receiver DSP flow is depicted in Fig. 2. After front-end correction, chromatic dispersion (CD) compensation and band de-multiplexing are realized by: converting the received signals to frequency domain by a long-tap FFT; multiplying by CD coefficients; using four short-tap IFFT to transfer each band to time domain. The subsequent per-sub-band DSP includes a multiple-input-multiple-output (MIMO) equalizer and carrier recovery to cope with the residual linear channel impairments and phase mismatch. The signal to interference

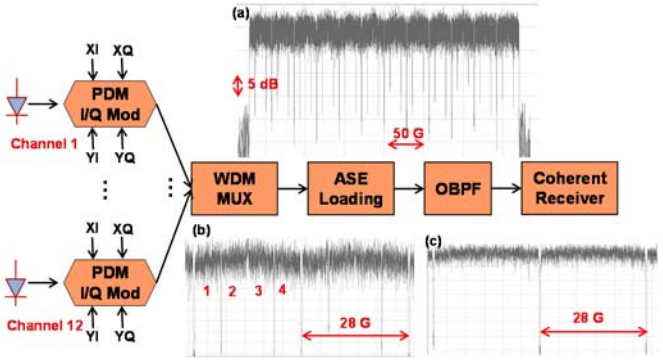

Fig. 4: Simulation setup. (a): spectrum of the entire superchannel; b): two channel spectrum with 4 sub-bands each channel; (c): two channel spectrum with single sub-band per channel.

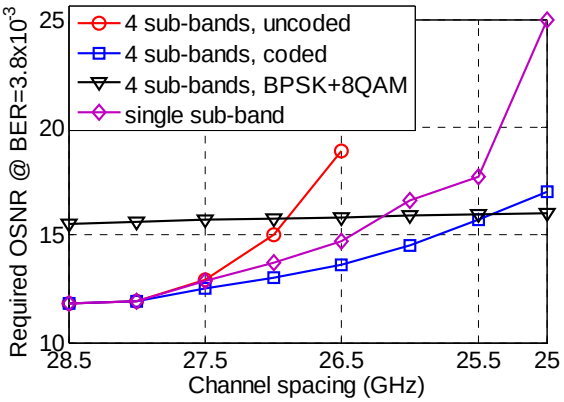

Fig. 5: Simulation results for different systems. Channel bandwidth of 28-GHz.

and noise ratio (SINR) is then estimated separately for each sub-band based on the constellation's statistical moments [20], which allows different linear rescaling of the equalized signals according to the estimated SINR (i.e., the signals are multiplied by the square root of SINR). Notably, the SINR difference may change due to varying ICI, therefore the SINR estimation should be updated periodically, e.g., in accordance to the laser drift rate. After I/Q de-interleaving, maximum likelihood detection (MLD) is used to make symbol decisions for BER calculation.

The essential idea of the sub-band pairwise coding is to transform the SINR difference between the paired sub-bands into the imbalance between the in-phase and quadrature components for both of the sub-bands, which enables the constellation rotation and rescaling to attain a better detection performance. Furthermore, with a fixed transmitter side design, this scheme is able to combat against varying fading values by updating the SINR estimation (rescaling factor) at the receiver.

III. System Verification

A. Simulation verification

We verified the effectiveness of sub-band pairwise coding in simulation using VPItransmissionMaker™. The simulation setup is shown in Fig. 4. The transmitted signal consisted of 12 channels, each at 28-GHz symbol rate. The channel spacing was set between 25 GHz to 28.5 GHz to simulate different laser-drift induced ICI levels. ASE noise at a 0.1 nm resolution bandwidth was loaded to test the system sensitivity. We compared four different systems: (1) single sub-band PDM-QPSK per channel, with spectrum shaped by a 0.01 roll-off root-raised-cosine (RRC) filter; (2) four sub-bands N-WDM PDM-QPSK system, each sub-band with a 7-GHz symbol rate; (3) pairwise coded four sub-band system, with 45° rotation angle; (4) four sub-bands system, using BPSK for the edge sub-bands and circular 8-QAM for the middle sub-bands, with equal power allocation for all sub-bands. The entire superchannel spectrum at a 28.5-GHz channel spacing is shown in Inset (a) of Fig. 4. The zoom-in of two channel spectra with four and single sub-band(s) per channel are depicted in the Insets (b) and (c) of Fig. 4, respectively. After a 40-GHz optical band pass filter (OBPF) to select the desired channel, a standard coherent receiver was used to detect the signals for receiver digital signal processing.

Figure 5 shows the required OSNR to achieve BER = 3.8×10^{-3} for the different systems. Clearly the 4 sub-bands uncoded system is more sensitive to increasing ICI than the single sub-band system, and its BER fails to fall below 3.8×10^{-3} when the channel spacing is less than 26.5 GHz. By applying sub-band pairwise coding, the ICI penalty can be largely mitigated for the 4 sub-band system, and less OSNR is required compared with the single sub-band system. This confirms the ICI advantage of sub-banding each channel and

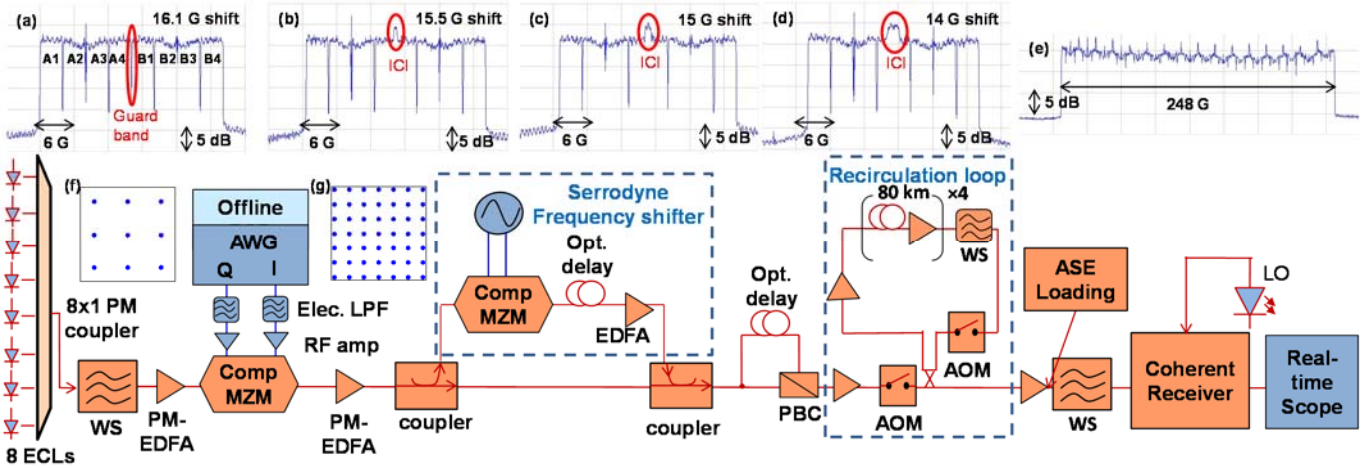

Fig. 6. Experimental setup for laser drift induced ICI mitigation, signal spectra are shown as the insets (a)-(e) (5dB/div vertical, 6GHz/div horizontal).

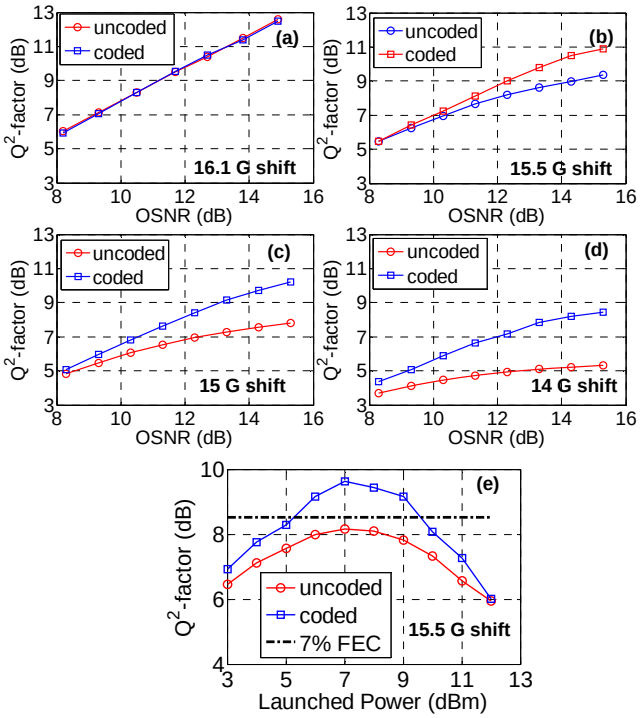

Fig. 7: Experimental results, using 4-sub-band QPSK channels: (a)-(d): B2B OSNR measurements, (e): results after 3840-km fiber with 15.5 GHz channel spacing.

applying this pre-coding technique. For the BPSK-8-QAM system, a static transmitter design is employed with equal powers in all of the sub-bands. It requires similar OSNR values with different ICI levels, because 75% of the bits are carried by the middle sub-bands that have no ICI, and BPSK was used in the edge sub-bands, which has higher resilience against ICI. The BPSK-8-QAM system achieves best performance when channel spacing is narrower than 25 GHz; however, it requires the highest OSNR when the channel overlap is less than 1 GHz. Therefore, optimal power allocation is necessary for this scheme to work efficiently over the time-varying ICI effects, *i.e.* the transmitter pre-coding needs to change adaptively using some feedback information; while sub-band pairwise coding is able to achieve a performance gain consistently without modifying the transmitter's rotation and interleaving process.

B. Experimental demonstration

Figure 6 shows the experimental setup of demonstrating sub-band pairwise coding against different laser-drift induced ICI levels. The transmitter comprised 8 external cavity lasers (ECLs), power-equalized by a Finisar Waveshaper (WS), and then modulated by electrical signals generated from an Agilent 64 GSa/s arbitrary waveform generator. A 16-Gbaud N-WDM signal with 4 sub-bands was generated per channel (4-Gbaud per sub-band), normal QPSK format were used for uncoded signals; with pairwise pre-coding at $\theta = 45^{\circ}$, the constellation becomes a 9-QAM like signal at each sub-band, as shown in Fig. 6(g). An odd-and-even superchannel structure was achieved by power-splitting the 8 modulated channels into two arms, delaying one arm and frequency shifting before recombining with the through arm. The signal was frequency

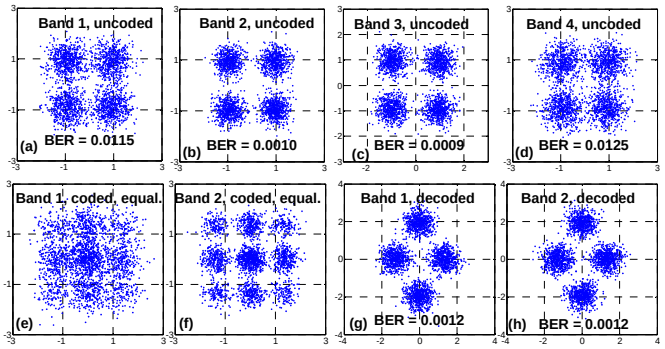

Fig. 8: Constellation diagrams of equalized signals with and without pairwise coding for QPSK transmission. Overlap of 0.5-GHz between channels.

shifted to modify the odd- and even-channel overlap, and the laser carrier frequency spacing was set to twice the frequency shift, resulting in different levels of ICI. The insets (a)-(d) of Fig. 6 show the spectra (captured by an Agilent 83453B) of a single channel and its frequency shifted version for 16.1-GHz, 15.5-GHz, 15-GHz and 14-GHz shifts, respectively. These shifts correspond to: a 100-MHz guard band, then 500-MHz, 1-GHz and 2-GHz channel overlaps, respectively. The ICI doubles when all channels are present. The 3-dB high peaks correspond to the spectrally overlapped channels (marked 'ICI'). Polarization-division-multiplexing was emulated by splitting the signals into two equal arms, delaying one arm and then recombining using a polarization beam combiner (PBC). The signals then passed through a fiber recirculating loop, consisting of two acousto-optic modulators, four 80-km spans of standard single mode fiber (SSMF), a WS for gain flattening and five erbium doped fiber amplifiers (EDFAs). The signal spectrum after 3840-km transmission with 15.5-GHz frequency shift is depicted as inset (e) of Fig. 6. The receiver consists of a WS for channel selection and a 25-GHz coherent receiver attached to a 40-GS/s real-time oscilloscope. ASE was added for back-to-back measurements. The offline DSP included front-end correction, resampling, frequency offset compensation, DFT operation, overlap-add band de-multiplexing with dispersion compensation, and per sub-band signal recovery with MIMO adaptive equalizer and phase estimation. Extra decoding was needed for the pairwise coded signals. For QPSK modulation, the constant modulus algorithm (CMA) [21] and a modified constant modulus algorithm (M-CMA) [22] were employed for the adaptive equalization of the un-coded and coded signals, respectively. Maximum likelihood phase estimation was applied for phase correction [23].

For B2B transmission, the measured Q^2-factor versus OSNR in 0.1-nm resolution is shown as Figs. 7(a)-(d) for different ICI cases. With a 16.1-GHz channel spacing, the coded and uncoded signals have similar performance, which illustrates that the pairwise coding does not introduce an extra penalty. When the spectral overlap is introduced and increased, the coded system shows much better performance than the uncoded system; with 15-dB OSNR, for 15.5/15/14 GHz spacing, the Q^2 penalty is 3.6/5.1/7.6 dB, while it reduces to 2/2.7/4.4 dB when pairwise coding is applied. Figure 7(e)

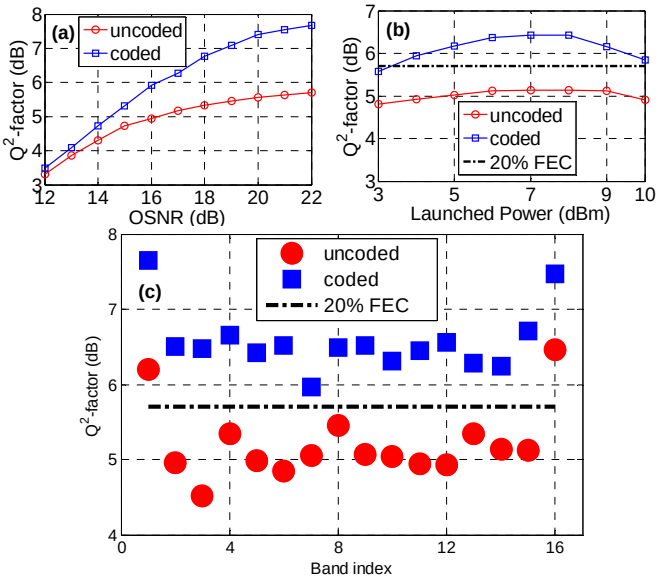

Fig. 9: 16-QAM results with 0.5-GHz overlap: (a) B2B OSNR measurements; (b) results with different launched powers after 800-km transmission; (c) performance for different channels after 800-km transmission with optimal launched power.

shows the performance of the 8th (centre) channel with 15.5-GHz spacing after 3840-km; the coded signals have an advantage of 1.5-dB Q^2 over the uncoded signals at the optimal launched power.

Figures 8(a)-(d) show the constellation diagrams of the equalized un-coded signals for sub-bands 1-4, respectively. Here again, the channel overlap is 0.5-GHz. Clearly, the BER is dominated by the edge (1 & 4) sub-bands. Figures 8(e)-(h) show the equalized coded signals for sub-bands 1 and 2. For a similar reason to the un-coded case, sub-band 1 has poorer SINR performance. After rescaling and I/Q de-interleaving, similar BERs can be observed for both sub-bands, as shown in Figs. 8(g) and (h). In this experiment, the in-phase component of the decoded signals of both sub-bands suffered more interference than the quadrature components, therefore the imaginary axis of the decoded signals has been 'stretched' to allow the two clusters sit on the imaginary axis further from the 'horizontal' noise from the two clusters that sit on the real axis.

We performed another experiment to test the effectiveness of proposed scheme with 16-QAM modulation format. All of the setup is the same as for QPSK, except that for the fiber link, every circulation loop consists of one span of 100-km fiber. The transmitter process was similar to QPSK; 45°-angle rotation was applied, leading to transmitted signal with 49 constellations points (Fig. 6(g)). The receiver DSP employed a dual-mode algorithm for the adaptive equalizer to converge [24]. The frequency shift was set to 15.5 GHz. Figure 8(a) shows the B2B OSNR measurements. More than 1.5-dB Q^2 improvement can be observed at 20-dB OSNR. The 800-km transmission performance with different launched powers is shown in Fig. 9(b); more than 1-dB enhancement is achieved at the optimal launched power. The performance of all channels after 800-km transmission is shown in Fig. 9(c); the edge channels have better performance because only one edge

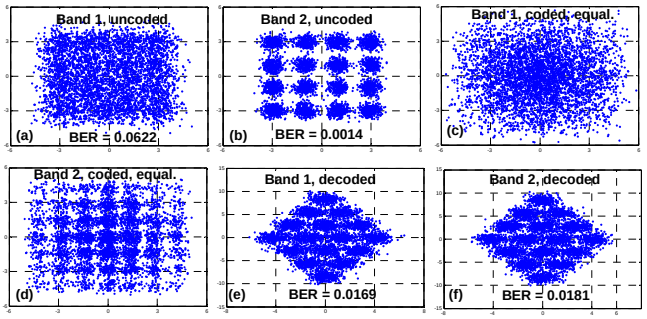

Fig. 10: Constellation diagrams of equalized signals with and without pairwise coding for 16-QAM transmission. 0.5-GHz overlap.

channel suffers severe ICI.

The recovered uncoded signals for Sub-bands 1 and 2 after 800-km transmission with optimal launch power are shown in Fig. 10(a) and (b), respectively. Figures 8(c)-(f) show the signals before and after pairwise decoding. As expected, after I/Q de-interleaving, each sub-band achieves similar BER, which is much smaller than the average BER in the uncoded system. Therefore, these results confirm that the proposed sub-band pairwise coding is able to operate with high-order QAM modulation formats.

IV. Conclusion

We have proposed employing sub-band pairwise coding for each wavelength channel, to improve the superchannel's robustness against ICI. The pre-coding process rotates the original signal constellation and interleaves the real and imaginary components between edge and middle sub-bands. At the receiver, after I/Q de-interleaving, the ICI imposed onto the edge sub-band translates into an SINR imbalance between I and Q components of both the edge and middle sub-bands. Therefore the subsequent rescaling process reduces the detection errors. Sub-band pairwise coding works for a static pre-coding process with a fixed 45° rotation angle, which greatly simplifies the transmitter implementation. Using a low-complexity decoder, the simulation and experimental results show that the proposed technique is able to adaptively mitigate random fast-varying ICI effects, and because of its low complexity, is highly suitable for practical deployment in future superchannel transceivers.

References

[1] P. J. Winzer, "Beyond 100G Ethernet," *IEEE Commun. Mag.*, vol. 48, no. 7, pp. 26–30, Jul. 2010.

[2] M. Camera, B. E. Olsson, and G. Bruno, "Beyond 100 Gbit/s: System implications towards 400 G and 1 T," in *Proc. ECOC Symp. Toward 1 Tb/s*, Torino, Italy, Sep. 2010, paper Th10G1.

[3] G. Bosco, A. Carena, V. Curri, P. Poggiolini, and F. Forghieri, "On the performance of Nyquist-WDM terabit superchannels based on PM-BPSK, PM-QPSK, PM-8QAM or PM-16QAM subcarriers," *J. Lightw. Technol.*, vol. 29, no. 1, pp. 53–61, Jan. 1, 2011.

[4] X. Zhou, J. Yu, M.-F. Huang, Y. Shao, T. Wang, L. Nelson, P. Magill, M. Birk, P. I. Borel, D. W. Peckham, and R. Lingle, "64-Tb/s (640 107-Gb/s) PDM-36QAM transmission over 320 km using both pre- and post-transmission digital equalization," in *Proc. Opt. Fiber Commun. Conf.*, San Diego, CA, 2010, Post-deadline paper PDPB9.

[5] C. Zhu, L. B. Du, B. Corcoran, A. V. Tran, T. Anderson, A. J. Lowery and E. Skafidas, "1.15 Tb/s Nyquist PDM 16-QAM transmission with

joint matched filtering and frequency-domain equalization," in *Proc. Opt. Fiber Commun. Conf.*, San Francisco, CA, 2014, Th4D.4.
[6] Y. Tang, W. Shieh, and B. S. Krongold, "DFT-Spread OFDM for fiber nonlinearity mitigation," *IEEE Photon. Technol. Lett.*, vol. 22, no. 16, pp. 1250–1252, Aug. 2010.
[7] L. B. Du, and A. J. Lowery, "Optimizing the subcarrier granularity of coherent optical communications systems," *Opt. Exp.*, vol. 19, no. 9, Apr. 2011.
[8] P. Poggiolini, A. Carena, Y. Jiang, G. Bosco, and F. Forghieri, "On the ultimate potential of symbol-rate optimization for increasing system maximum reach," in *Proc. Eur. Conf. Opt. Conf.*, Valencia, Spain, 2015, We.4.6.2.
[9] C. Liu, J. Pan, T. Detwiler, A. Stark, Y.-T. Hsueh, G.-K. Chang, and S. E. Ralph, "Joint digital signal processing for superchannel coherent optical communication systems," *Opt. Express*, vol. 21, no. 7, pp. 8342–8356, 2013 .
[10] B. S. Krongold, K. Ramchandran, and D. L. Jones, "Computationally efficient optimal power allocation algorithms for multicarrier communication systems," *IEEE Trans. Commun.*, vol. 48, pp. 23–27, Jan. 2000.
[11] J.-C. Belfiore, G. Rekaya, and E. Viterbo, "The Golden code: A 2 2 full-rate space-time code with nonvanishing determinants," *IEEE Trans. Inf. Theory*, vol. 51, no. 4, pp. 1432–1436, Apr. 2005.
[12] O. Tirkkonen and A. Hottinen, "Square-matrix embeddable space-time block codes for complex signal constellations," *IEEE Trans. Inf. Theory*, vol. 48, pp. 1122–1126, Feb. 2002.
[13] S. K. Mohammed, E. Viterbo, Y. Hong, and A. Chockalingam, "MIMO precoding with X- and Y-codes," *IEEE Trans. Inf. Theory*, Nov. 2010.
[14] Y. Hong, A. J. Lowery, and E. Viterbo, "Sensitivity improvement and carrier power reduction in direct-detection optical OFDM systems by subcarrier pairing," *Opt. Express*, vol. 20, no. 2, pp. 1635–1648, 2012.
[15] C. Zhu, B. Song, L. Zhuang, B. Corcoran, and A. J. Lowery, "Pairwise Coding to Mitigate Polarization Dependent Loss," in *Proc. Opt. Fiber Commun. Conf.*, Los Angeles, CA, 2015, W4K.4.
[16] C. Zhu, B. Song, B. Corcoran, L. Zhuang, and A. J. Lowery, "Improved polarization dependent loss tolerance for polarization multiplexed coherent optical systems by polarization pairwise coding," *Opt. Express*, vol.23, no.21, pp. 27434-27447, 2015.
[17] C. Zhu, B. Song, L. Zhuang, B. Corcoran, and A. J. Lowery, "Sub-band pairwise coding for inter-channel-interference mitigation in superchannel transmission systems," in *Proc. Eur. Conf. Opt. Conf.*, Valencia, Spain, 2015, Tu.3.4.3.
[18] J. Boutros and E. Viterbo, "Signal space diversity: A power- and bandwidth-efficient diversity technique for the Rayleigh fading channel," *IEEE Trans. Inform. Theory*, vol. 44, pp. 1453–1467, July 1998.
[19] L. B. Du, C. Zhu, B. Foo, J. Schroder, and A. J. Lowery, "DAC generated multi-channel Nyquist WDM," in *Proc. OECC*, Melbourne, Australia, 2014, MO2B-1.
[20] C. Zhu, A. V. Tran, S. Chen, L. B. Du, C. C. Do, T. Anderson, A. J. Lowery, and E. Skafidas, "Statistical moments based OSNR monitoring for coherent optical systems," *Opt. Express*, vol. 20, no. 16, pp. 17711-17721, Jul. 2012.
[21] S. J. Savory, "Digital filters for coherent optical receivers," *Opt. Express*, vol. 16, no. 2, 804-817 (2008).
[22] J. Zhang, J. Yu, N. Chi, Z. Dong, J. Yu, X. Li, L. Tao, and Y. Shao, "Multi-modulus blind equalizations for coherent quadrature duobinary spectrum shaped PM-QPSK digital signal processing," *J. Lightw. Technol.*, vol. 31, no. 7, pp. 1073–1078, Apr. 1, 2013.
[23] S. Zhang, P.-Y. Kam, C. Yu, and J. Chen, "Decision-aided carrier phase estimation for coherent optical communications" *J. Lightwave Technol.*, vol. 28, no. 17, pp. 1597-1607, Jun. 2010.
[24] C. Zhu, A. V. Tran, S. Chen, L. B. Du, T. Anderson, A. J. Lowery, and E. Skafidas, "Frequency-domain blind equalization for long-haul coherent pol-mux 16-QAM system with CD prediction and dual-mode adaptive algorithm," *IEEE Photon. J.*, vol. 4, no. 5, pp. 1654-1661, Oct. 2012.

Chen Zhu (S'10–M'14) received the Master of Telecommunication degree and the Ph.D. degree in electrical and electronic engineering from the University of Melbourne, Parkville, Australia, in 2010 and 2014, respectively. In 2012, he was an intern for half a year at the optical transmission department, European Research Center, Huawei Technologies, Munich, Germany. In 2014 he was awarded the IEEE photonics society student fellowship. He is currently a Research Fellow with the Melbourne Electro-Photonics Lab, Electrical and Computer Systems Engineering, Monash University, Melbourne, Australia. His current research interests include high-speed short-reach and long-haul optical systems design, digital signal processing, and optical signal processing.

Binhuang Song (S'14) received the B.Sc. degree (with first-class honors) in Electronic communication system & Photonics from the Australian National University (ANU), Canberra, Australia, and Beijing Institute of Technology, Beijing, China, in 2014. He is currently working toward the Ph.D. degree with the Electro-Photonics Laboratory at Monash University. Mr. Song was a recipient of the Monash Graduate Scholarship for the duration of his Ph.D. degree.

Leimeng Zhuang (S'05–M'10) was born in Beijing, China, in 1980. He received the B. Sc. Degree in telecommunication engineering from the Univeristy of Electronic Science and Technology of China, Chengdu, China, in June 2003, and the M. Sc. Degree in electrical engineering (Hons.) and Ph.D. degree in electrical engineering, both from the Univeristy of Twente, Enschede, The Netherlands, in June 2005 and November 2010, respectively. His Ph.D. thesis was about the true time delay-based broadband phased array antenna system comprising a photonic integrated beamformer using tunable ring resonator delay lines. From October 2009 until September 2010, he worked as a Product Specialist at XiO Photonics B.V., mainly involved in photonics integration and packaging. In the period from October 2010 until December 2013, he worked as a Research Fellow at the University of Twente, SATRAX B.V., and Dutch National Aerospace Laboratory, responsible for the development of a satellite tracking phased array antenna system. In March 2014, he joined the Electro-Photonics Laboratory, Electrical and Computer Systems Engineering, Monash University in Melbourne, Australia. He is currently a research fellow, working on the topic of hybrid platform combining electronics and photonics for high-speed, energy-efficient optical communication systems and microwave photonics.

Bill Corcoran (S'07–M'xx) received the degrees of B.Sc and B.Eng(Hons) from RMIT University (Melbourne, Australia), and PhD from the University of Sydney (Sydney, Australia) in 2006 and 2011, respectively. His PhD work focused on enhanced optical nonlinearities in silicon waveguides. Following this, he worked on phase-sensitive amplification at Chalmers University of Technology (Gothenburg, Sweden)

from 2011-2013. Since 2013, he has worked within the Electro-Photonics Laboratory at Monash University (Melbourne, Australia) as part of the Australian Research Council's Centre for Ultrahigh-bandwidth Devices for Optical Systems (CUDOS), and became a member of faculty within the Department of Electrical and Computer Systems Engineering in 2015. His current research interests include topics around the themes of optical super-channels, nonlinear optical transmission and optically routed networks.

Arthur J. Lowery (M'92–SM'96–F'09) was born in Yorkshire, U.K., in 1961. He received the B.Sc. degree (with first class honors) in applied physics from the University of Durham, Durham, U.K., in 1983 and the Ph.D. degree in electrical and electronic engineering from the University of Nottingham, Nottingham, U.K., in 1988. From 1983 to 1984, he was with Marconi Radar Systems Ltd., U.K. In 1984, he joined the University of Nottingham as a lecturer and pioneered time domain field modeling of semiconductor lasers as the Transmission-Line Laser Model. In 1990, he joined the University of Melbourne, Australia. In 1996, he co-founded Virtual Photonics Pty. Ltd. (now VPIphotonics) and led to the development of VPIs physical-level photonic design automation tools. In 2004, he was appointed as a Professor with the Department of Electrical and Computer Systems Engineering, Monash University, Melbourne and was head between 2007 and 2012. In 2008, he founded Ofidium to commercialize optical OFDM for long-haul systems. In 2009, he was elected an IEEE Fellow for leadership in computer modeling of optical communication systems. He is currently Director of the Monash Vision Group's Bionic Eye project and Science Leader of Tbit/s Systems in the ARC's Centre of Excellence in Ultrahigh bandwidth Devices for Optical Systems (CUDOS), and Chief Investigator in the Centre for Integrative Brain Function. He has published more than 250 papers. In 2007 he was awarded the Clunies Ross Award from the Australian Academy of Technological Sciences and Engineering (ATSE) for his work at VPIsystems. In July 2013, he was awarded a five-year ARC Laureate Fellowship to work on electro-photonic interchanges.